Rotational scanning and multiple-spot focusing through a multimode fiber based on digital optical phase conjugation

Chaojie Ma[1], Jianglei Di[1], Ying Li[1], Fajun Xiao[1], Jiwei Zhang[1], Kaihui Liu[2]*, Xuedong Bai[3], and Jianlin Zhao[1]*

[1]MOE Key Laboratory of Material Physics and Chemistry under Extraordinary Conditions, and Shaanxi Key Laboratory of Optical Information Technology, School of Science, Northwestern Polytechnical University, Xi'an 710072, China
[2]State Key Laboratory for Mesoscopic Physics, School of Physics, Peking University, Beijing 100871, China
[3]China Institute of Physics, Chinese Academy of Sciences, Beijing 100080, China

*E-mail: khliu@pku.edu.cn; jlzhao@nwpu.edu.cn

We demonstrate, for the first time, the rotational memory effect of a multimode fiber (MMF) based on digital optical phase conjugation (DOPC) to achieve multiple-spot focusing. An implementation interferometer is used to address the challenging alignments in DOPC. By rotating the acquired phase conjugate pattern, rotational scanning through a MMF could be achieved by recording a single off-axis hologram. The generation of two focal spots through a MMF is also demonstrated by combining the rotational memory effect with the superposition principle. The results may be useful for ultrafast scanning imaging and optical manipulation of multiple objects through a MMF. © 2018 The Japan Society of Applied Physics

Controlling light propagation through or inside scattering media is critically important in many application fields, such as imaging and communication.[1,2] When light encounters scattering media, such as white paint and biological tissue, multiple scattering events occur that seriously impede light focusing and imaging. The process of multiple elastic scattering is seemingly complex and random but actually linear and deterministic, and can be fully described by using a scattering transmission matrix.[3] The pioneers in this research field have exploited these linear and deterministic properties to overcome the multiple scattering by iterative wavefront shaping,[4,5] measuring the transmission matrix,[3] and optical phase conjugation (OPC).[6–11] Among these methods, the OPC based on the principle of time reversal requires the shortest average response time per degree of freedom. It can be divided into two categories: analog OPC and digital OPC (DOPC). Unlike analog OPC-based nonlinear crystals or effects,[6–8] DOPC is based on a digital image sensor and a spatial light modulator (SLM). Here, the sensor is used to acquire a scattered wavefront by digital holography, and the SLM serves to generate the phase conjugate wavefront.[9–11] Thus, DOPC has several intrinsic advantages, such as freely working in a broad wavelength range, effectively achieving higher phase conjugate reflectivity, and flexibly adjusting the original phase conjugate wavefront.[12–14]

At present, endoscopic imaging, for which fiber bundles composed of thousands of individual cores are widely used owing to their simplicity, is an important tool for industry and biomedical science.[15–17] However, conventional fiber bundles suffer from a limited spatial resolution owing to the diameter of the individual cores and the core-to-core spacing.[16] Although some higher resolution methods have been proposed, the requirement for a large number of individual cores for high-resolution imaging has caused a restriction on the cross section of the endoscope.[18,19] Recently, multimode fibers (MMFs) have attracted intense attention owing to their minimal cross section and large capacity for light information delivery and collection.[16,17] However, as the light beam propagates through a MMF, it will be distorted into a speckle field because of modal scrambling. Fortunately, it is shown that the random process is linear, and mode scrambling can be overcome by wavefront shaping methods, such as iterative

wavefront optimization,[20,21] transmission matrix measurement,[22–24] and DOPC.[25,26] Compared with the two other methods, DOPC does not require iterative optimization of the wavefront or determination of the elements of the transmission matrix, and thus could potentially offer the shortest response time.

Light propagation through scattering media shows the angular memory effect where tilting the incident wavefront over small angles maintains a high degree of correlation in the resulting speckle field.[2] In recent years, the angular memory effect has been actively developed for fast scanning and noninvasive wide-field imaging.[10,27,28] However, the angular memory effect is absent in MMFs owing to their special geometry. In contrast to conventional scattering media, MMFs feature cylindrical symmetry[24] and show the rotational memory effect, which was exploited in conjunction with iterative wavefront optimization.[29,30] However, it only demonstrated the achievement of rotational scanning and was time-consuming, owing to the need for multiple iterations.

In this paper, we demonstrate the exploitation of the rotational memory effect in conjunction with DOPC for not only achieving rotational scanning, but also generating multiple focal spots through a MMF, simultaneously with a single shot. The implementation interferometer shows a trapezoid Sagnac-like ring feature,[31,32] which is inspired by the setup for wide-field imaging using DOPC in Ref. 32. Employing this interferometer, we can overcome the implementation-challenging alignments in DOPC.[9,32,33] Then, we demonstrate the achievement of light focusing through a MMF by recording a single off-axis hologram. Finally, on the basis of the rotational memory effect, we demonstrate the achievement of rotational scanning within a certain rotation angle limited by the partial cylindrical symmetry of the used MMF. On this basis, we further develop the rotational memory effect in conjunction with the superposition principle to generate two focal spots.

Figure 1 shows the experimental setup of DOPC with a trapezoid Sagnac-like ring feature to achieve light focusing through a MMF. The laser source is a diode-pumped solid-state laser with a wavelength of 532 nm. The laser beam is expanded and collimated via a microscope objective (MO_1) (Newport M-20x, NA = 0.4), a pinhole of 15 μm, and a lens (L_1). The collimated beam travels through a half-wave plate
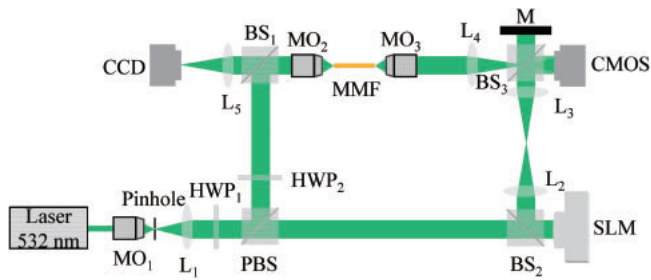
Fig. 1. Experimental setup for DOPC with a trapezoid Sagnac-like ring feature. MO_1–MO_3: microscope objectives; L_1–L_5: lenses; HWP_1, HWP_2: half-wave plates; PBS: polarized beam splitter; BS_1–BS_3: beam splitters; M: mirror.

Fig. 2. Experimental results of addressing the relative spatial displacement between the SLM and CMOS. (a) Periodic pattern displayed on SLM. (b) Measured intensity image using CMOS.

(HWP_1) to adjust its polarization state and then is split into two beams with orthogonal polarizations by a polarized beam splitter (PBS). The vertically polarized beam through another half-wave plate (HWP_2) is changed into a horizontally polarized one, and then it is reflected by a beam splitter (BS_1) into a microscope objective (MO_2) (Newport M-40x, NA = 0.65). After that, it is coupled into the front facet of a step index MMF (18 cm length, 105 μm core diameter, NA = 0.22 ± 0.02) and generates a speckle field at the output facet. The speckle field is imaged on the target of a CMOS camera (MotionBLITZ EoSens Cube7) through a microscope objective (MO_3) (Newport M-40x, NA = 0.65) and a lens (L_4). The horizontally polarized beam is incident on a reflective phase-only SLM (Holoeye Pluto-Vis) to achieve phase-only modulation. The beam subsequently reflected from the SLM mounted on a self-assembly six-dimensional stage through a beam splitter (BS_2), a $4f$ imaging system composed of lenses L_2 and L_3, and a beam splitter (BS_3) is imaged on the CMOS target. Finally, the two beams (acting as an object beam and a reference beam) interfere with each other on the CMOS target to form an off-axis hologram. The interferogram visibility is adjusted with the HWP_1. By the angular spectrum method, the recorded hologram is reconstructed to acquire amplitude and phase information of the speckle field.[34,35] The phase information of the speckle field is first linearly calculated in grayscale and then projected on the phase-only SLM to generate the phase conjugate wavefront, which propagates in the reverse direction through the MMF after being reflected by the mirror M positioned in the imaging plane of the SLM. Finally, the phase conjugate focal spot is observed using a CCD through an imaging system composed of MO_2 and L_5.

Despite DOPC's significant potential, its practical applications are limited by two major challenging alignment problems. One is that the SLM and image sensor must be precisely aligned pixel-to-pixel and the other is that the phase conjugate wavefront and original scattering wavefront must be strictly overlapped.[32,33] The precise alignments are significant to the final efficiency of DOPC. Here, we first address the relative spatial displacement between the SLM and CMOS by using a $4f$ imaging system. The region of interest of the CMOS is set to 800×800 pixels, and the writeable region of the SLM is also set to 800×800 pixels and then divided into 50×50 sections with 16×16 pixels in each section. The phase differences between adjacent sections are set to π. Figure 2(a) shows the periodic pattern displayed on the SLM. As the reference beam is incident on the SLM, the beam reflected from the SLM is modulated by the
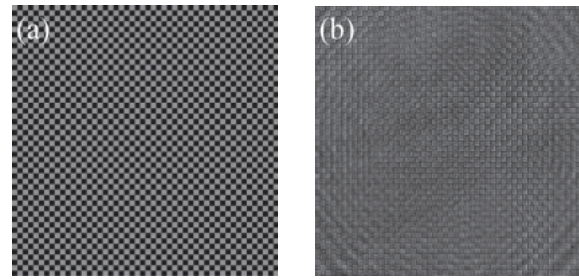
periodic pattern. When the object beam is blocked, the reflected beam carrying the periodic pattern information is imaged on the region of interest of the CMOS target through the $4f$ imaging system, as shown in Fig. 2(b), with mechanical adjustment. In such a way, we have addressed the spatial misalignment between the SLM and CMOS. Next, we must ensure precise overlap between the phase conjugate wavefront and the original scattering wavefront to achieve DOPC. The difficulty is transformed into challenging alignments in six misalignment dimensions between the mirror M and SLM. In fact, in-plane misalignments between the mirror M and SLM, including in-plane translation and rotation misalignments, do not exist. Moreover, the axis translation misalignment could be overcome by placing the mirror M in the equivalent plane of the CMOS with the mechanical adjustment. Therefore, we only need to consider the tilt/tip parameters, which could be autocorrected by the angular spectrum method, to precisely overlap the phase conjugate wavefront and the original scattering wavefront at the location of the MMF facet.[33–35]

First, we investigate the excitation spot close to the fiber axis. The speckle field is formed at the fiber output facet and interferes with the reference beam on the CMOS target. When the grayscale values of the pattern displayed on the SLM are set to 0, an off-axis hologram is recorded using the CMOS camera, as shown in Fig. 3(a). The intensity and phase information of the speckle field reconstructed by the angular spectrum method are shown in Figs. 3(b) and 3(c), respectively. The phase information of the speckle field is linearly calculated in grayscale and then projected on the SLM. As the phase conjugate pattern is displayed on the SLM and the reference beam is incident on the SLM, the beam reflected from the SLM carries the phase conjugate wavefront, which is delivered back to the MMF after being reflected by mirror M. The original scattering wavefront and phase conjugate wavefront are precisely overlapped in the MMF by autocorrecting the tilt/tip parameters by the angular spectrum method. Finally, when the object beam is blocked, the phase conjugate focal spot is recorded using the CCD, as shown in Fig. 3(d). The intensity profile of the focal spot along the horizontal direction is shown in Fig. 3(e). The full width at half-maximum (FWHM) is 1.30 μm, which is limited by the numerical aperture of the MMF. To evaluate the DOPC performance, the speckle pattern is recorded when no phase conjugation pattern is displayed on the SLM, as shown in Fig. 3(f). The peak-to-background ratio (PBR), defined as the ratio between the peak intensity of the focal spot and the
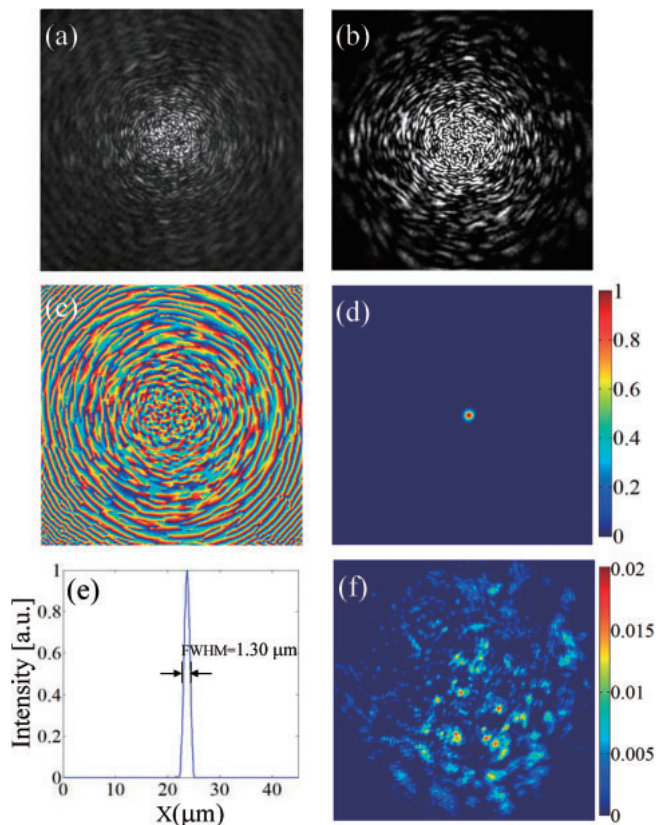
Fig. 3. Experimental results of focusing through a MMF using DOPC. (a) Recorded hologram. (b) Reconstructed speckle pattern. (c) Phase information of the speckle field. (d) Phase conjugate focal spot. (e) Intensity profile of the focal spot. (f) When the CCD exposure time is extended 20 times, the speckle pattern is recorded using the CCD as no phase conjugation pattern is displayed on the SLM.
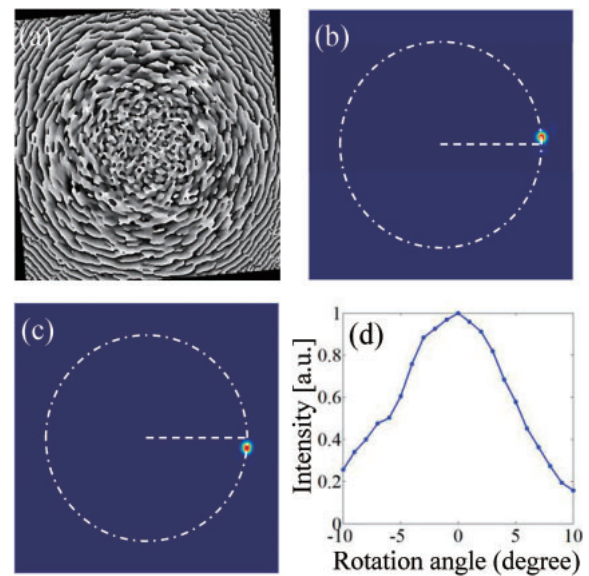

Fig. 4. Experimental results for rotational scanning by exploiting the rotational memory effect in a MMF. (a) Phase conjugate pattern displayed on the SLM. (b, c) Phase conjugate focal spots. (d) Variation in intensity maximums of the focal spots during rotation.

mean intensity of a speckle field generated when no phase conjugation pattern is displayed on the SLM, is about 900.

In contrast to conventional scattering media, the angular memory effect is absent in MMFs. Nevertheless, MMFs feature cylindrical symmetry and show the rotational memory effect, which was exploited to achieve rotational scanning by the iterative wavefront shaping method.[29,30] However, the method used needs multiple iterations, which is time-consuming. Here, we exploit the rotational memory effect in conjunction with DOPC to achieve rotational scanning through a MMF by recording a single off-axis hologram. The range of the rotational memory effect precisely depends on the position of the fiber axis.[30] Thus, we first determine the position of the fiber axis by imaging the fiber output facet on the CMOS target. In addition, the symmetry of the MMF itself seriously affects the speckle correlation coefficient during rotation.[24,30] Here, we investigate the excitation spot deviated from the fiber axis. To demonstrate the rotational memory effect, we rotate the original phase conjugate pattern around the fiber axis by a bilinear interpolation procedure. Figures 4(a) and 4(b) show the phase conjugate pattern displayed on the SLM rotated clockwise an angle of $-5°$ and the conjugate focal spot recorded using the CCD, respectively. For comparison, Fig. 4(c) depicts the recorded focal spot when the phase conjugate pattern rotated clockwise an angle of $5°$ on the SLM. Owing to the partial cylindrical symmetry of the MMF used, the memory effect in the rotational range of $\pm 10°$ is feasible. The variation in intensity

maximums of the focal spots is shown in Fig. 4(d). Although the focal spot intensity decreases as the rotation angle increases, the focal spots are still brighter than the background. Actually, if the MMF has perfect cylindrical symmetry, rotational scanning over a full range of angles could be achieved. Therefore, the demonstrated results could be expected to provide an approach for ultrafast scanning imaging through a MMF.

Multiple-spot focusing through a MMF was demonstrated by measuring the transmission matrix, which was used for holographic tweezers and fluorescent imaging, for example.[22,24] However, the transmission matrix measurement requires iterative determination of the elements, which is time-consuming. Here, we develop the rotational memory effect in conjunction with the superposition principle,[36] which was not exploited and could be used for generating multiple focal spots through a MMF with a single shot. Considering the partial cylindrical symmetry of the MMF used, here, we only demonstrate the simultaneous generation of two focal spots. We also investigate the excitation spot deviated from the fiber axis. Two phase conjugate patterns are acquired by rotating the original phase conjugate pattern for two different angles. These two patterns are superposed to synthesize one phase conjugate pattern. Figure 5(a) shows the synthesized phase conjugate pattern displayed on the SLM, from two superposed phase conjugate patterns rotated clockwise for angles of $\pm 5°$. When the phase conjugate wavefront propagates in the reverse direction, two focal spots are simultaneously generated and recorded using the CCD, as shown in Fig. 5(b). The distance between the two focal spots can be adjusted within the range of the effective memory effect of the MMF. Figures 5(c) and 5(d) show the two focal spots generated when the synthesized phase conjugate patterns comprise two superposed phase conjugate patterns rotated clockwise for angles of $\pm 6°$, and $\pm 7°$, respectively. As can be seen in Figs. 5(b)–5(d), the distances between the two focal spots clearly increase.
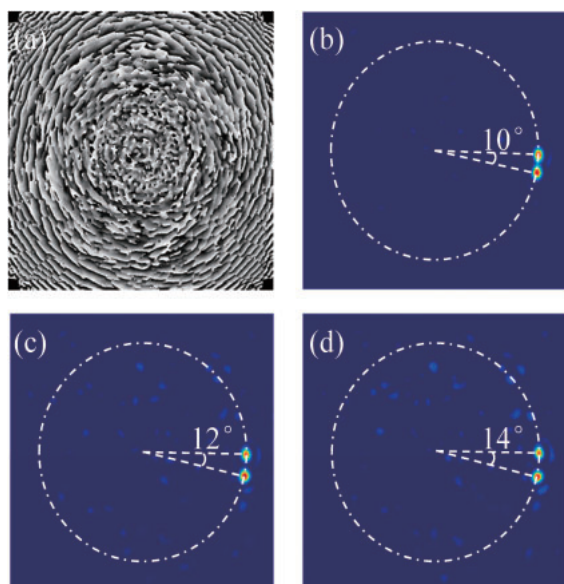
Fig. 5. Experimental results for two-spot focusing through a MMF. (a) Synthesized phase conjugate pattern. (b)–(d) Two focal spots generated through a MMF when different synthesized phase conjugate patterns are displayed on the SLM.

We have demonstrated a method of achieving rotational scanning and multiple-spot focusing through a MMF by combining the rotational memory effect with DOPC. The employment of the interferometer with a trapezoid Sagnac-like ring feature can overcome the challenging alignment constraints in DOPC and only the tilt/tip parameters need be autocorrected by the angular spectrum method. By rotating the acquired phase conjugation pattern around the fiber axis within a certain range limited by the partial cylindrical symmetry of the MMF used, rotational scanning through a MMF has been successfully achieved with a single shot. Moreover, we have further achieved the generation of two focal spots through a MMF by exploiting the rotational memory effect in conjunction with the superposition principle. Actually, rotational scanning over the full range of angles and more focal spots can be achieved as long as the MMFs show perfect cylindrical symmetry. This method offers high potential for applications such as ultrafast scanning imaging, wide-field endoscopic imaging, and optical manipulation.

1) A. P. Mosk, A. Lagendijk, G. Lerosey, and M. Fink, Nat. Photonics **6**, 283 (2012).
2) S. Rotter and S. Gigan, Rev. Mod. Phys. **89**, 015005 (2017).
3) S. M. Popoff, G. Lerosey, R. Carminati, M. Fink, A. C. Boccara, and S. Gigan, Phys. Rev. Lett. **104**, 100601 (2010).
4) I. M. Vellekoop and A. P. Mosk, Opt. Lett. **32**, 2309 (2007).
5) I. M. Vellekoop, A. Lagendijk, and A. P. Mosk, Nat. Photonics **4**, 320 (2010).
6) Z. Yaqoob, D. Psaltis, M. S. Feld, and C. Yang, Nat. Photonics **2**, 110 (2008).
7) X. Xu, H. Liu, and L. V. Wang, Nat. Photonics **5**, 154 (2011).
8) Q. Gao, Z. Lu, C. Zhu, and J. Zhang, Appl. Phys. Express **8**, 052501 (2015).
9) M. Cui and C. Yang, Opt. Express **18**, 3444 (2010).
10) C. L. Hsieh, Y. Pu, R. Grange, G. Laporte, and D. Psaltis, Opt. Express **18**, 20723 (2010).
11) I. M. Vellekoop, M. Cui, and C. Yang, Appl. Phys. Lett. **101**, 081108 (2012).
12) B. Judkewitz, Y. M. Wang, R. Horstmeyer, A. Mathy, and C. Yang, Nat. Photonics **7**, 300 (2013).
13) C. Ma, X. Xu, Y. Liu, and L. V. Wang, Nat. Photonics **8**, 931 (2014).
14) Y. Shen, Y. Liu, C. Ma, and L. V. Wang, Opt. Lett. **41**, 1130 (2016).
15) B. A. Flusberg, E. D. Cocker, W. Piyawattanametha, J. C. Jung, E. L. M. Cheung, and M. J. Schnitzer, Nat. Methods **2**, 941 (2005).
16) G. Oh, E. Chung, and S. H. Yun, Opt. Fiber Technol. **19**, 760 (2013).
17) H. Yu, J. Park, K. Lee, J. Yoon, K. Kim, S. Lee, and Y. Park, Curr. Appl. Phys. **15**, 632 (2015).
18) D. Kim, J. Moon, M. Kim, T. D. Yang, J. Kim, E. Chung, and W. Choi, Opt. Lett. **39**, 1921 (2014).
19) N. Stasio, C. Moser, and D. Psaltis, Opt. Lett. **41**, 3078 (2016).
20) R. Di Leonardo and S. Bianchi, Opt. Express **19**, 247 (2011).
21) T. Čižmár and K. Dholakia, Opt. Express **19**, 18871 (2011).
22) S. Bianchi and R. Di Leonardo, Lab Chip **12**, 635 (2012).
23) Y. Choi, C. Yoon, M. Kim, T. D. Yang, C. Fang-Yen, R. R. Dasari, K. J. Lee, and W. Choi, Phys. Rev. Lett. **109**, 203901 (2012).
24) T. Čižmár and K. Dholakia, Nat. Commun. **3**, 1027 (2012).
25) I. N. Papadopoulos, S. Farahi, C. Moser, and D. Psaltis, Opt. Express **20**, 10583 (2012).
26) I. N. Papadopoulos, S. Farahi, C. Moser, and D. Psaltis, Opt. Lett. **38**, 2776 (2013).
27) I. M. Vellekoop and C. M. Aegerter, Opt. Lett. **35**, 1245 (2010).
28) O. Katz, P. Heidmann, M. Fink, and S. Gigan, Nat. Photonics **8**, 784 (2014).
29) L. V. Amitonova, A. P. Mosk, and P. W. H. Pinkse, Opt. Express **23**, 20569 (2015).
30) S. Rosen, D. Gilboa, O. Katz, and Y. Silberberg, arXiv:1506.08586.
31) C. Ma, Y. Li, J. Zhang, P. Li, T. Xi, J. Di, and J. Zhao, Opt. Express **25**, 13659 (2017).
32) T. R. Hillman, T. Yamauchi, W. Choi, R. R. Dasari, M. S. Feld, Y. Park, and Z. Yaqoob, Sci. Rep. **3**, 1909 (2013).
33) M. Jang, H. Ruan, H. Zhou, B. Judkewitz, and C. Yang, Opt. Express **22**, 14054 (2014).
34) J. Zhang, C. Ma, S. Dai, J. Di, Y. Li, T. Xi, and J. Zhao, Opt. Lett. **41**, 3844 (2016).
35) C. Ma, J. Di, J. Zhang, Y. Li, T. Xi, E. Li, and J. Zhao, Appl. Opt. **55**, 9435 (2016).
36) J. Ryu, M. Jang, T. J. Eom, C. Yang, and E. Chung, Sci. Rep. **6**, 23494 (2016).